Au/TS-1 Catalyst Prepared by Deposition-Precipitation Method for Propene Epoxidation with H_2/O_2: Insights into the Effects of Slurry Aging Time and Si/Ti Molar Ratio

Xiang Feng[a], Xuezhi Duan[a], Hongye Cheng[a], Gang Qian[a], De Chen[b], Weikang Yuan[a], Xinggui Zhou[a,*]

[a] *State Key Laboratory of Chemical Engineering, East China University of Science and Technology, 130 Meilong Road, Shanghai 200237, China*

[b] *Department of Chemical Engineering, Norwegian University of Science and Technology, Trondheim 7491, Norway*

Abstract: Au/TS-1 catalyst prepared by deposition-precipitation method is efficient for propene epoxidation with H_2/O_2, and its performance is significantly affected by the preparation parameters and the properties of support. In this work, effects of the slurry aging time and Si/Ti ratio of support on the location of Au nanoparticles inside or outside the micropores of TS-1 supports are examined by multi-techniques such as in-situ characterization and molecular dynamic simulation, and the as-obtained catalysts are tested for propene epoxidation. It is found that longer slurry aging time facilitates the evolution of Au complex into smaller-sized species which is easier to locate inside the micropores. Accordingly, the as-reduced catalyst has more tiny Au nanoparticles that are extremely active inside micropores and shows higher initial PO formation rate ($g_{PO}h^{-1}g_{Au}^{-1}$). In addition, high Si/Ti ratio of TS-1 also favors the deposition of Au nanoparticles inside micropores, resulting in higher initial activity but lower stable activity.

Keywords: Propene epoxidation; Aging time; Si/Ti molar ratio; Au location; Catalytic performance

*Corresponding author. Tel.: +86-21-64253509. Fax.: +86-21-64253528. E-mail address: xgzhou@ecust.edu.cn

1 Introduction

Propylene oxide (PO) is an important bulk chemical intermediate for producing a variety of derivatives such as polyurethane foams, resins and propylene glycol. Compared with traditional chlorohydrin and several organic hydroperoxide processes, direct propene epoxidation with molecular H_2 and O_2 to PO provides a greener, simpler and more sustainable route [1, 2]. For this reaction, the synergy between Au nanoparticles and isolated Ti^{4+}-containing supports is indispensable because the synthesized H_2O_2 by H_2 and O_2 on Au nanoparticles should transfer to nearby isolated Ti^{4+} sites to form Ti-OOH, which is responsible for the oxidation of propene to PO [3-6]. Therefore, Au/Ti-containing catalysts (e.g., Au/TS-1) that are prepared by deposition-precipitation (DP) method show excellent catalytic performance [5-22], because the Au nanoparticles could be selectively deposited close to the active titanium sites rather than the inactive silicon sites when the pH of solution is higher than the isoelectric point of silicon sites [6].

To date, considerable and successful efforts have been devoted to improving the performance of the Au/TS-1 catalysts by optimizing the DP process [7, 21-25]. For example, Delgass et al. reported that, compared with cesium hydroxide and ammonium hydroxide, Na_2CO_3 was a better neutralizing agent for Au catalyst preparation [26]. Lu et al. showed that the pH of the solution would affect the Au loading efficiency, and a pH of 7 is better for the catalyst towards PO synthesis [24]. Lee and Zanella et al. reported that the aging time of Au and support slurry in DP process is critical to the catalytic performance of Au catalysts [27, 28]. Recently, Delgass et al. showed that by prolonging the slurry aging time from 1 to 10 h, the initial PO formation rate of Au/TS-1 catalyst increased from ca. 80 to 160 $g_{PO}h^{-1}kg_{Cat}^{-1}$ at 200 ^oC, which was

possibly because the contact time between the support and Au complexes affects the active sites for PO formation [22]. This catalyst was shown to have the highest activity without adding any promoters. However, mechanistic insights into the effect of slurry aging time on the structural properties and performance of Au catalysts are desired to the rational design of more effective Au/Ti-containing catalysts for direct propene epoxidation.

The Si/Ti molar ratio is also reported to have significant influence on the DP process and catalytic performance of Au catalysts [13, 22, 24, 25]. For example, Oyama et al. reported that different Si/Ti molar ratio could affect Au capture efficiency in the DP process [24]. Delgass et al. showed that the optimum Si/Ti molar ratio was 100 [7, 21, 22]. However, this result is not consistent with the previous understanding of Haruta et al. [13, 25, 29] that a low Si/Ti molar ratio (e.g. 36) of Au/titanosilicalite catalyst will result in a higher activity because the in situ generated hydroperoxy complexes can be more efficiently utilized. To date, this debate still remains unresolved [22] and in-depth understanding on the effect of Si/Ti molar ratio on structural properties of Au catalysts is still lacking.

It is well known that in the DP process, chloroauric acid, which is a widely used Au precursor, evolves into different forms that have different sizes and affinities to the support [27, 30]. When the slurry aging time and the Si/Ti molar ratio of the support are varied, the composition of Au complexes and their interactions with supports may be different. It is expected that completely different structural properties such as size and location of Au nanoparticles on the internal or external surfaces of support will be obtained, and the catalytic performance will also be different. Therefore, understanding the effects of these variables will undoubtedly be beneficial to improving the

performance of the Au/TS-1 catalyst for PO synthesis.

The present work aims to understand the effect of Au slurry aging time and the Si/Ti molar ratio of TS-1 support on Au location and the performance of Au/TS-1 catalyst for propene epoxidation. We first use in-situ UV-vis and molecular dynamics simulations to study the composition and size of Au complexes at different lengths of aging time, and then use HRTEM, XPS and N_2 physisorption to determine the size and the location of the Au nanoparticles on the support. It is revealed that longer aging time of Au slurry and higher Si/Ti molar ratio of support enable small-sized Au complexes with smaller mass transfer resistance to easily enter into the micropores of support. As a result, the reduced catalyst has more highly active Au nanoparticles inside the micropores and thus exhibits higher initial PO formation rate but faster deactivation due to micropore blocking. The insights reported here not only unravel the effect of slurry aging time and Si/Ti molar ratio of support on Au location both experimentally and theoretically, but also resolve the reported controversial issue of optimum Si/Ti molar ratio of Ti-containing supports.

2 Experimental

2.1 Synthesis of TS-1 supports and Au/TS-1 catalysts

Titanium silicalite-1 (TS-1) supports with different Si/Ti molar ratios were synthesized according to the previously published procedure [22, 31]. A typical process began with the addition of 3.5 g polyoxyethylene 20-sorbitan monolaurate (Tween 20, Aldrich) to 45 mL deionized water, which was followed by drop-wise addition of a mixture of 44.8 g tetrapropylammonium hydroxide (TPAOH, 25 wt%) and 66.4 g tetraethylorthosilicate (TEOS, 95 wt%). The solution was vigorously stirred at room

temperature for more than 0.5 h. Titanium (IV) tetrabutoxide (TBOT, 99 wt%) dissolved in 20 mL isopropanol (WAKO, 99.5 wt%) was then added drop-wise. The final solution was further stirred for over 1 h and crystallized in a Teflon autoclave at 423 K for over 18 h. The as-synthesized solid was thoroughly washed with deionized water and dried overnight at room temperature, followed by calcination at 823 K for 5.5 h to remove the TPA template. The obtained TS-1 supports are designated according to the Si/Ti molar ratio. For example, a TS-1 sample with a Si/Ti molar ratio of 100 is designated TS-1(100). Au/TS-1 catalysts were prepared by the deposition-precipitation (DP) method outlined in our previous reports [4-6]. Besides, 0.5 g TS-1 was mixed with 0.1 g $HAuCl_4 \cdot 3H_2O$ and 50 mL H_2O for 30 min. Subsequently, the pH of Au and TS-1 slurry was adjusted to 7.3-7.5 by 1 M NaOH and maintained for different hours to tune the Au loading. The solid was then centrifuged for 30 min, washed twice with deionized water and dried at 28 ^oC under vacuum. The slurry aging time mentioned in this work represents the time maintained at the pH of 7.3-7.5.

2.2 Catalyst characterization and quench molecular dynamics simulations

The crystal phases of the TS-1 supports were characterized by X-ray diffraction (XRD, Rigaku D/Max2550VB/PC, Cu K_α radiation). The types of Au complexes were determined by in situ ultraviolet-visable spectroscopy which was recorded on a spectrometer (AvaSpec-2048) equipped with a transmission dip probe. The pore diameters and pore volumes of the Au/TS-1 catalysts were measured by nitrogen at 77 K with Micromeritics ASAP2020 instrument. Each sample was degassed at 523 K for 4 h, and then analyzed for 3 days to obtain the complete adsorption-desorption isotherm. The Au loadings were determined by atomic absorption spectroscopy (AAS, ZEEnit 600). The high-resolution transmission electron microscopy (HRTEM) images were

obtained on a JEOL JSM-2010. The metal particle sizes and distributions were determined by measuring more than 150 randomly selected particles. The chloride ion concentration was examined by ion chromatography (Dionex 600). The surface Au/Si molar ratios were determined by X-ray photoelectron spectroscopy (XPS) on a Kratos XSAM-800 instrument using Al K_α X-ray with 1486.6 eV as the excitation source.

Quench molecular dynamics simulation was conducted to obtain the stable structures of Au complexes. Materials Studio package and the Universal Force Field was used for this purpose and the simulation was conducted at 298 K in the microcanonical ensemble (NVE). A time step of 1 fs was adopted, and the total simulation time was 100 ps. Geometry optimization calculations were performed every 5 ps. By comparing the energies of the quenched structures, the lowest energy conformation of Au complexes was identified.

2.3 Catalytic testing

The performance of the catalyst for gas-phase propene epoxidation was carried out at normal pressure in a quartz tubular reactor (i.d. 8 mm) using 0.15 g catalyst of 60-80 mesh particle size. The feed concentration was fixed at 10/10/10/70 vol.% of C_3H_6, H_2, O_2 and N_2 (at a space velocity of 14,000 $mLh^{-1}g_{cat}^{-1}$) . The reactor was heated from room temperature to 200 ^oC for reaction. The concentration of reactants and products were measured online by two gas chromatographs (Agilent 6890) equipped with TCD (Porapak Q and 5A columns) and FID (Porapak T column) detectors.

3 Results and discussion

3.1 Effect of slurry aging time

UV-vis spectroscopy is a powerful tool to characterize the evolution of Au complexes at different lengths of aging time. Fig. 1a shows the UV-vis spectra of Au complexes at different pH levels. At pH of 2.2, there are two intense adsorption bands assigned to the ligand-to-metal charge transfer transitions from chlorine *p* to gold *d* orbitals. The two bands at ca. 240 and 313 nm are associated with $p_\sigma \rightarrow d_{x^2-y^2}$ and $p_\pi \rightarrow d_{x^2-y^2}$ transitions, respectively [32, 33]. At a higher pH level, the Au complexes hydrolyze with the exchange of chloride for hydroxyl ions. This leads to the blue-shift and the decreased intensity of the bands, which are in accordance with the results of Baatz et al. [34]. Table 1 shows the composition of Au complexes (e.g., $[AuCl_4]^-$, $[AuCl_3(OH)]^-$, $[AuCl_2(OH)_2]^-$, $[AuCl(OH)_3]^-$) at different pH levels [35, 36]. From the spectra (Fig. 1a) and compositions of Au complexes (Table 1) at different pH levels, it is possible to monitor the composition of Au complexes at different lengths of aging time. Fig. 1b shows the in situ UV-vis spectra of Au complexes as a function of aging time, during which the pH was kept at 7.3-7.5. The composition of Au complexes changes very slowly with time, and the establishment of hydrolysis equilibrium requires a long time, as indicated by the slow blue-shift of the main adsorption band in the initial 16 h. In this process, Au precursors evolve into extensively hydrolyzed Au complexes such as $[AuCl(OH)_3]^-$ and $[Au(OH)_4]^-$ that have less Cl ions.

(Fig. 1 should be inserted here)

(Table 1 should be inserted here)

Fig. 2 shows the lowest energy conformations of different Au complexes obtained from the quench molecular dynamics simulations. For the five Au complexes, the simulated bond distances of Au-Cl and Au-O are found to be 2.26 Å and 1.88 Å,

respectively, which approximate the Au-Cl and Au-O bond distances of 2.26 and 1.98 Å determined via X-ray absorption spectroscopy [37]. The size of each Au complex (L) is calculated by $L = L_{AB} + r_A + r_B$, where L_{AB} is the distance between the two furthest atoms (A and B), and r_A and r_B are the covalent radii of A and B atoms, respectively. For example, the calculated longest distance in $[AuCl_4]^-$ complex is the length between two Cl atoms (i.e., 4.53 Å) and the covalent radius of Cl atom is 0.99 Å [38]. Therefore, the size of $[AuCl_4]^-$ is 4.53+0.99*2=6.51 Å. The calculated sizes of all the Au complexes decrease in the order of $[AuCl_4]^- > [AuCl_3(OH)]^- = [AuCl_2(OH)_2]^- > [AuCl(OH)_3]^- > [Au(OH)_4]^-$ (see Table 2). It is noted that the calculated sizes of $[AuCl_3(OH)]^-$ and $[AuCl_2(OH)_2]^-$ are the same. However, the steric hindrance of $[AuCl_3(OH)]^-$, which has more chloride ions, can be larger than that of $[AuCl_2(OH)_2]^-$. In addition, $[Au(OH)_4]^-$ can easily enter into the micropores of TS-1 because of its smaller size than the diameter of the microporous channels (ca. 0.55 nm). Other Au complexes may also enter into the micropores by stretching and bending vibrations [39, 40] but with greater difficulties. In general, the more extensively hydrolyzed Au complexes are easier to enter into the micropores of the TS-1 support because of its smaller size and steric hindrance. It should be noted that Bond et al. proposed the existence of $Au(OH)_3$ from $[Au(OH)_4]^-$ and H_2O [35], though Zanella et al. did not observed it by XAS [28]. If it does exist, it is formed in the solution after a longer aging time when $[Au(OH)_4]^-$ has been formed. Its small size of 0.51 nm, smaller than $[AuCl_4]^-$, $[AuCl_3(OH)]^-$, $[AuCl_2(OH)_2]^-$ and $[AuCl(OH)_3]^-$, indicates it is easy to locate in the micropores of TS-1, resulting in a decrease in microporous volume.

(Fig. 2 should be inserted here)

(Table 2 should be inserted here)

TS-1 supports with Si/Ti molar ratios of 35 and 100 are prepared by typical hydrothermal method for the deposition of Au complexes. On their XRD patterns shown in Fig. 3a, there is only a single peak at ca. 24.5^{o}, which is assigned to the presence of orthorhombic unit cell. These patterns coincide with the reported typical MFI structure of TS-1, and indicate the high crystalline purity of the two TS-1 supports [31]. Fig. 3b displays the N_2 adsorption-desorption isotherms of TS-1(35) and TS-1(100) supports. The typical type I isotherms, according to the IUPAC classification, show that the two TS-1 supports are microporous materials [41]. Both of the samples exhibit peaks centering at ca. 5.5 Å on the pore size distribution (PSD) curves (Fig. 3b). In addition, the TS-1(35) and TS-1(100) supports also have similar micropore volumes of 0.162 and 0.156 cm^3g^{-1}, respectively. The incorporation of titanium into the MFI framework is confirmed by the characteristic bands of framework Ti species at 960 cm^{-1} in the FT-IR spectra (Fig. 3c) [42, 43]. The type of Ti complexes in the framework of the support is characterized by UV-vis spectroscopy, and the results are shown in Fig. 3d. Both samples have the main adsorption peak at 220 nm, which is ascribed to the charge transfer from O^{2-} to Ti^{4+} and is characteristic of isolated tetrahedally coordinated Ti ion in the framework [41, 44, 45]. The higher adsorption intensity at 220 nm for TS-1(35) than that for TS-1(100) is because of the higher Ti content in the framework of TS-1(35). The absence of adsorption peaks at 260 and 330 nm indicates the absence of octahedrally coordinated Ti complexes and anatase phase, respectively. The above results show that the two supports have similar physico-chemical properties, i.e., microporous and highly crystalline structure, and the only existence of isolated Ti^{4+} in the framework.

(Fig. 3 should be inserted here)

Table 3 shows the properties of TS-1(100) and Au/TS-1(100) samples prepared at different lengths of slurry aging time. With the increase of aging time from 4 to 10 h, the micropore volume of Au/TS-1(100) catalysts reduces from 0.145 to 0.125 cm^3g^{-1}. The change of microporous volumes of pure TS-1 supports at pH of 7.3~7.5 for different aging time is neglected, indicating that the change of microporous volume is only affected by Au clusters. The reduction in micropore volume is smaller in early hours than in late hours. From 4 to 8 h, the micropore volume is reduced by only 0.005 cm^3g^{-1}, while from 8 to 10 h, the volume is reduced by 0.015 cm^3g^{-1}. This is consistent with the calculated results that the Au complexes after a longer aging time are easier to enter into the microporous channels of TS-1. The micropore volume decreases from 0.125 to 0.118 cm^3g^{-1} when the aging time is extended from 10 to 18 h, indicating that more extensively hydrolyzed Au complexes enter into the micropores of support. When the aging time is further increased from 18 to 24 h, the micropore volume increases, instead of decreases, from 0.118 to 0.135 cm^3g^{-1}. This is because the dominant complex at this time is $[Au(OH)_4]^-$ which has the smallest adsorption constant [27, 30] and could be easily removed from TS-1 micropores under vigorous stirring. Correspondingly, the Au loading decreases from 0.139 to 0.120 wt%.

(Table 3 should be inserted here)

Table 4 shows the bulk and surface composition of Au/TS-1(100) samples. It is noted that the Au clusters tend to locate on the external surfaces of microprous TS-1 support, as indicated by the slightly higher surface Au/Si molar ratio than the bulk Au/Si molar ratio. To find the tendency of Au clusters to locate at the internal or external surfaces of the support, normalized surface Au/Si molar ratio is calculated by dividing the surface Au/Si molar ratio by Au loading. It is shown that when the slurry aging time is increased from 4 to 24 h, the normalized surface Au/Si molar ratio decreases from

0.91 to 0.46. This shows that Au clusters tend to locate inside the micropores of TS-1 at a longer aging time.

(Table 4 should be inserted here)

Fig. 4 shows the PO formation rates per gram of Au of Au/TS-1(100) catalysts prepared at different lengths of aging time. By prolonging the aging time from 4 to 24 h, the PO formation rate per gram of Au first increases from 149 to 163 $g_{PO}h^{-1}g_{Au}^{-1}$ and then decreases to 100 $g_{PO}h^{-1}g_{Au}^{-1}$. This is not due to the effect of chloride ions [46] and oxidation state of Au because the chloride ion concentration of the samples after washing is negligible (i.e., lower than 5 ppm). For Au/TS-1 catalysts, the PO formation rate is significantly affected by the particle size of Au on the internal (i.e., inside the micropores) and external surfaces of TS-1 [5, 6, 21-23, 47]. Fig. 5 shows the observable Au average particle sizes on the external surfaces of Au/TS-1 catalysts at lengths of aging time of 4, 18 and 24 h. The Au average particle size of Au/TS-1 catalyst with an aging time of 10 h is 3.0 nm, as has been shown in our previous work [6]. From 4 to 10 h, the observable Au average particle size increases from 2.7 to 3.2 nm. However, there are more tiny Au clusters inside micropores that could hidden from view by HRTEM at aging time of 10 h (Table 3, 4). The smaller Au clusters inside the microporous channels of TS-1 are much more active towards PO formation than Au nanoparticles on the external surfaces. This has been demonstrated by Delgass et al. and our group using TS-1/Silicate-1 composite and uncalcined TS-1, respectively [5,21]. As a result, with the contribution of more active tiny Au clusters inside microporous channels, the PO formation rate of Au catalyst at aging time of 10 h (163 $g_{PO}h^{-1}g_{Au}^{-1}$) is higher than that of the Au catalyst at the aging time of 4 h (i.e., 149 $g_{PO}h^{-1}g_{Au}^{-1}$). Further increasing the aging time of slurry from 10 to 18 h allows more extensively hydrolyzed Au complexes to enter into the micropores. However, too many Au clusters inside the micropores may

also make those deep inside the microspores not easily accessible by reactants. The pore diffusion resistance will become significant because of the narrowed pore size. This results in the decrease of PO formation rate from 163 to 110 $g_{PO}h^{-1}g_{Au}^{-1}$. When the aging time keeps increasing from 18 to 24 h, the PO formation rate decreases to 90 $g_{PO}h^{-1}g_{Au}^{-1}$ because less Au nanoparticles (Table 3) are inside the microporous channels and the average Au particles size on the external surfaces of TS-1(100) support (Fig. 5d) becomes larger. It can also be seen from Fig. S1 that the H_2 efficiency decreases by prolonging the aging time from 4 to 24 h, which is due to larger Au nanoparticles on the external surfaces of TS-1(Fig. 5). On larger Au nanoparticles, H_2O_2 diffuses a longer way to reach the Ti site for epoxidation and has more chances to decompose [5].

(Fig. 4 should be inserted here)

(Fig. 5 should be inserted here)

3.2 Effect of Si/Ti molar ratio

When the Si/Ti molar ratio of support is varied, the affinity of the Au complex towards the TS-1 surface and thus the Au capture efficiency will be different, which can affect the structural properties and catalytic performance of Au/TS-1 catalysts. For a convenient comparison of the catalytic performance, the Au loadings of Au/TS-1(35) and Au/TS-1(100) catalysts were kept the same of 0.10 wt%. The slurry aging time for Au/TS-1(100) catalyst (i.e., 10 h) is longer than that for Au/TS-1(35) catalyst (i.e., 6 h) (Fig. S2). The lower Au capture efficiency of TS-1(100) support is mainly due to its lower Ti content since Au nanoparticles are selectively deposited near the titanium sites of the support [6]. Table 5 shows the properties of the TS-1 and the Au/TS-1 with different Si/Ti molar ratios. The micropore volumes of both TS-1(35) and TS-1(100) supports decrease after deposition of Au. Nevertheless, the reduced micropore volumes

are different. For 0.10 wt% Au/TS-1(100) catalyst, the reduction of micropore volume (i.e., 0.031 $cm^3 \cdot g^{-1}$) is larger than 0.021 $cm^3 \cdot g^{-1}$ for 0.10 wt% Au/TS-1(35), demonstrating that the portion of Au clusters inside the microporous channels of 0.10 wt% Au/TS-1(100) catalyst is larger than that of 0.10 wt% Au/TS-1(35) catalyst. This is mainly because on TS-1(100) support, the rate of Au adsorption is smaller and the mass transfer resistance is less important. The longer aging time of 10 h allows more Au complexes with smaller steric hindrance to enter into the micropores of the TS-1(100) support (Fig. 6).

(Table 5 should be inserted here)

(Fig. 6 should be inserted here)

Fig. 7 shows the catalytic performance of 0.10 wt% Au/TS-1(100) and 0.10 wt% Au/TS-1(35) catalysts. In our previous work, we elucidated the effect of Si/Ti molar ratio by using uncalcined TS-1 with blocked micropores (TS-1-B) supported Au catalysts to exclude the contribution of Au clusters inside micropores. It is found that smaller Si/Ti molar ratio about 35 favors the PO formation [4]. However, 0.10 wt% Au/TS-1(100) catalyst shows higher initial PO formation rate than 0.10 wt% Au/TS-1(35) catalyst in this work. It is noteworthy that compared to the 0.10 wt% Au/TS-1(35) catalyst, the 0.10 wt% Au/TS-1(100) catalyst has more Au clusters inside the microporous channels and similar average Au particle sizes on the external surfaces (Fig. S3). Therefore, the higher PO formation rate of Au/TS-1(100) in this work indicates that the apparent effect of Si/Ti molar ratio of TS-1 on the performance of the Au/TS-1 catalyst is entangled by the location of the Au clusters inside or outside the micropores [4-7, 48]. This result further explains the controversial issue concerning the optimum Si/Ti molar ratio (i.e., 35 or 100) in literature [13, 22, 25, 29], which is

virtually affected by not only the Si/Ti molar ratio of support but also the number of tiny Au clusters inside the microporous channels.

(Fig. 7 should be inserted here)

It is also observed in Fig. 7 that 0.10 wt% Au/TS-1(100) catalyst suffers from more severe deactivation. The deactivation of microporous TS-1 supported Au catalyst is mainly caused by micropore blocking [5, 6]. Under reacting conditions, the microporous channels will be partly blocked by some carbonaceous deposits, rendering the Au clusters in the micropores hardly accessible to the reactants [6]. Consequently, these Au clusters do not function as well as the nanoparticles on the external surface of the TS-1 support. Therefore, with more Au clusters inside the microproes, the 0.10 wt% Au/TS-1(100) catalyst suffers from more severe deactivation and exhibits lower stable activity than the 0.10 wt% Au/TS-1(35) catalyst. To achieve both high activity and stability, depositing tiny Au nanoparticles on nano-sized hierarchical TS-1with enhanced mass transfer is an interesting topic and will be carried out in our future work.

4 Conclusions

In summary, we have elucidated both experimentally and theoretically the effect of slurry aging time and Si/Ti molar ratio of support on the Au location (i.e., inside or outside micropores of TS-1). It is found that Au complexes at longer slurry aging time will evolve into smaller forms and become easier to locate inside the micropores of the TS-1(100) support. Consequently, the as-reduced Au/TS-1(100) catalysts have more highly active Au nanoparticles inside the micropores and thus show higher initial activities in terms of the PO formation rate per gram of gold. However, further increasing the slurry aging time results in too many Au clusters inside the micropores, which on the contrary reduce the activity possibly due to the pore diffusion resistance.

In addition, the TS-1(100) support has smaller Au capture efficiency than TS-1(35) support, and requires longer slurry aging time (ca. 10 h) to achieve the same Au loading of 0.10 wt% than that of TS-1(35) (ca. 6 h). The longer aging time allows more Au complexes with smaller steric hindrance to enter into the micropores of the support. This results in a higher initial activity of 0.10 wt% Au/TS-1(100) catalyst but faster deactivation caused by micropore blocking. This work might shed new light on the design of highly effective Au catalysts for PO formation.

Acknowledgments

This work is financially supported by the 973 Program (2012CB720501) and the 111 Project of Ministry of Education of China (B08021).

References

[1] T. Hayashi, K. Tanaka and M. Haruta, J. Catal. 178 (1998) 566-575.
[2] J. Huang, T. Takei, T. Akita, H. Ohashi and M. Haruta, Appl. Catal. B 95 (2010) 430-438.
[3] J.J. Bravo-Suarez, K.K. Bando, J. Lu, M. Haruta, T. Fujitani and T. Oyama, J. Phys. Chem. C 112 (2008) 1115-1123.
[4] X. Feng, X. Duan, J. Yang, G. Qian, X. Zhou, D. Chen and W. Yuan, Chem. Eng. J. (2014).
[5] X. Feng, X. Duan, G. Qian, X. Zhou, D. Chen and W. Yuan, J. Catal. 317 (2014) 99-104.
[6] X. Feng, X. Duan, G. Qian, X. Zhou, D. Chen and W. Yuan, Appl. Catal. B 150 (2014) 396-401.
[7] W.-S. Lee, M. Cem Akatay, E.A. Stach, F.H. Ribeiro and W. Nicholas Delgass, J. Catal. 308 (2013) 98-113.
[8] L. Xu, Y. Ren, H. Wu, Y. Liu, Z. Wang, Y. Zhang, J. Xu, H. Peng and P. Wu, J. Mater. Chem. 21 (2011) 10852-10858.
[9] H. Yang, D. Tang, X. Lu and Y. Yuan, The J. Phys. Chem. C 113 (2009) 8186-8193.
[10] J. Lu, X. Zhang, J.J. Bravo-Suárez, K.K. Bando, T. Fujitani and S.T. Oyama, J. Catal. 250 (2007) 350-359.
[11] G. Qian, Y.H. Yuan, W. Wu and X.G. Zhou, Stud. Surf. Sci. Catal. 159 (2006) 333-336.
[12] Y.-H. Yuan, X.-G. Zhou, W. Wu, Y.-R. Zhang, W.-K. Yuan and L. Luo, Catal. Today 105 (2005) 544-550.
[13] A.K. Sinha, S. Seelan, T. Akita, S. Tsubota and M. Haruta, Appl. Catal. A 240 (2003) 243-252.
[14] B.S. Uphade, T. Akita, T. Nakamura and M. Haruta, J. Catal. 209 (2002) 331-340.
[15] G. Mul, A. Zwijnenburg, B. van der Linden, M. Makkee and J.A. Moulijn, J. Catal. 201 (2001) 128-137.
[16] T.A. Nijhuis, B.J. Huizinga, M. Makkee and J.A. Moulijn, Ind. Eng. Chem. Res. 38 (1999) 884-891.

[17] M. Du, G. Zhan, X. Yang, H. Wang, W. Lin, Y. Zhou, J. Zhu, L. Lin, J. Huang, D. Sun, L. Jia and Q. Li, J. Catal. 283 (2011) 192-201.
[18] A.K. Sinha, S. Seelan, S. Tsubota and M. Haruta, Angew. Chem. Int. Ed. 43 (2004) 1546-1548.
[19] W.-S. Lee, M. Cem Akatay, E.A. Stach, F.H. Ribeiro and W. Nicholas Delgass, J. Catal. 313 (2014) 104-112.
[20] J. Chen, E.A. Pidko, V.V. Ordomsky, T. Verhoeven, E.J. Hensen, J.C. Schouten and T.A. Nijhuis, Catal. Sci. Tech. 3 (2013) 3042-3055.
[21] W.-S. Lee, L.-C. Lai, M. Cem Akatay, E.A. Stach, F.H. Ribeiro and W.N. Delgass, J. Catal. 296 (2012) 31-42.
[22] W.-S. Lee, M. Cem Akatay, E.A. Stach, F.H. Ribeiro and W. Nicholas Delgass, J. Catal. 287 (2012) 178-189.
[23] J. Huang, E. Lima, T. Akita, A. Guzmán, C. Qi, T. Takei and M. Haruta, J. Catal. 278 (2011) 8-15.
[24] J. Lu, X. Zhang, J.J. Bravo-Suárez, T. Fujitani and S.T. Oyama, Catal. Today 147 (2009) 186-195.
[25] B. Taylor, J. Lauterbach and W.N. Delgass, Appl. Catal. A 291 (2005) 188-198.
[26] E.E. Stangland, B. Taylor, R.P. Andres and W.N. Delgass, J. Phys. Chem. B 109 (2005) 2321-2330.
[27] S.-J. Lee and A. Gavriilidis, J. Catal. 206 (2002) 305-313.
[28] R. Zanella, S. Giorgio, C.R. Henry and C. Louis, J. Phys. Chem. B 106 (2002) 7634-7642.
[29] C. Qi, T. Akita, M. Okumura, K. Kuraoka and M. Haruta, Appl. Catal. A 253 (2003) 75-89.
[30] Y.A. Nechayev and N. Nikolenko, Geochem. Int. 23 (1986) 142-146.
[31] R.B. Khomane, B.D. Kulkarni, A. Paraskar and S.R. Sainkar, Mater. Chem. Phys. 76 (2002) 99-103.
[32] A.K. Gangopadhayay and A. Chakravorty, J. Chem. Phys. 35 (2004) 2206-2209.
[33] J.A. Peck, C.D. Tait, B.I. Swanson and G.E. Brown Jr, Geochim. Cosmochim. Acta 55 (1991) 671-676.
[34] C. Baatz, N. Decker and U. Prüße, J. Catal. 258 (2008) 165-169.
[35] F. Moreau and G.C. Bond, Catal. Today 122 (2007) 260-265.
[36] Y.A. Nechayev and N. Nikolenko, Geochem. Int 23 (1986) 142-146.
[37] X. Chen, W. Chu, D. Chen, Z. Wu, A. Marcelli and Z. Wu, Chem. Geol. 268 (2009) 74-80.
[38] P. Pyykkö and M. Atsumi, Chem. Eur. J. 15 (2009) 186-197.
[39] H. Schmidbaur, H.G. Raubenheimer and L. Dobrzańska, Chem. Soc. Rev. 43 (2014) 345-380.
[40] M. Maity, S. Das and N.C. Maiti, Phys. Chem. Chem. Phys. 16 (2014) 20013-20022.
[41] Z. Wang, L. Xu, J.-g. Jiang, Y. Liu, M. He and P. Wu, Microporous Mesoporous Mater. 156 (2012) 106-114.
[42] P. Wu, T. Tatsumi, T. Komatsu and T. Yashima, J. Phys. Chem. B 105 (2001) 2897-2905.
[43] A. Zecchina, S. Bordiga, C. Lamberti, G. Ricchiardi, D. Scarano, G. Petrini, G. Leofanti and M. Mantegazza, Catal. Today 32 (1996) 97-106.
[44] D. Serrano, R. Sanz, P. Pizarro, I. Moreno and S. Medina, Appl. Catal. B 146 (2014) 35-42.
[45] E. Duprey, P. Beaunier, M.-A. Springuel-Huet, F. Bozon-Verduraz, J. Fraissard, J.-M. Manoli and J.-M. Brégeault, J. Catal. 165 (1997) 22-32.
[46] A. Hugon, N.E. Kolli and C. Louis, J. Catal. 274 (2010) 239-250.
[47] X. Lu, G. Zhao and Y. Lu, Catal. Sci. Tech. 3 (2013) 2906-2909.
[48] J. Chen, S.J.A. Halin, E.A. Pidko, M.W.G.M. Verhoeven, D.M.P. Ferrandez, E.J.M. Hensen, J.C. Schouten and T.A. Nijhuis, ChemCatChem 5 (2013) 467-478.

Table captions:

Table 1. The composition of Au complexes at different pH levels [36].

Table 2 The calculated sizes of different Au complexes.

Table 3 The properties of TS-1(100) and Au/TS-1(100) samples.

Table 4 Surface and bulk composition of Au/TS-1(100) samples.

Table 5 Properties of TS-1 and Au/TS-1 samples with different Si/Ti molar ratios.

Table 1. The composition of Au complexes at different pH levels [36].

pH of Au solution	Existing Au complexes
0-1	$[AuCl_4]^-$
1-3	$[AuCl_4]^-$, $[AuCl_3(OH)]^-$
3-4	$[AuCl_4]^-$, $[AuCl_3(OH)]^-$, $[AuCl_2(OH)_2]^-$
4-5	$[AuCl_4]^-$, $[AuCl_3(OH)]^-$, $[AuCl_2(OH)_2]^-$, $[AuCl(OH)_3]^-$
5-6	$[AuCl_3(OH)]^-$, $[AuCl_2(OH)_2]^-$, $[AuCl(OH)_3]^-$
6-8	$[AuCl_2(OH)_2]^-$, $[AuCl(OH)_3]^-$, $[Au(OH)_4]^-$
8-10	$[AuCl(OH)_3]^-$, $[Au(OH)_4]^-$
>10	$[Au(OH)_4]^-$

Table 2 The calculated sizes of different Au complexes.

Au complexes	Size (Å)
$[AuCl_4]^-$	6.51
$[AuCl_3OH]^-$	6.50
$[AuCl_2(OH)_2]^-$	6.50
$[AuCl(OH)_3]^-$	5.81
$[Au(OH)_4]^-$	4.90

Table 3 The properties of TS-1(100) and Au/TS-1(100) samples.

Sample	Aging time (h)	Au loading (%)	V_{MP}[a] (cm^3g^{-1})
TS-1(100)	-	-	0.156
TS-1(100)	4	-	0.154
TS-1(100)	18	-	0.152
TS-1(100)	25	-	0.152
Au/TS-1(100)	4	0.067	0.145
Au/TS-1(100)	8	0.079	0.140
Au/TS-1(100)	10	0.100	0.125
Au/TS-1(100)	18	0.139	0.118
Au/TS-1(100)	24	0.120	0.135

[a] Micropore volume (V_{MP}) is estimated by t-plot method.

Table 4 Surface and bulk composition of Au/TS-1(100) samples.

Sample	Aging time (h)	Au loading (%)	Bulk Au/Si molar ratio (10^{-4})[a]	Surface Au/Si molar ratio(10^{-4})[b]	Normalized surface Au/Si molar ratio[c]	Average diameter of Au (nm)
Au/TS-1(100)	4	0.067	2.2	4.69	0.70	2.7
Au/TS-1(100)	10	0.100	3.4	5.54	0.55	3.0
Au/TS-1(100)	18	0.139	4.6	7.00	0.45	3.2
Au/TS-1(100)	24	0.120	4.2	5.54	0.46	3.8

[a] Bulk Au/Si molar ratio is determined by ICP analysis.

[b] Surface Au/Si molar ratio is determined by XPS analysis.

[c] Normalized Surface Au/Si molar ratio is determined by dividing the surface Au/Si molar ratio by Au loading.

Table 5 Properties of TS-1 and Au/TS-1 samples with different Si/Ti molar ratios.

Sample	Au loading (wt%)	Aging time (h)	V_{MP}[a] ($cm^3 \cdot g^{-1}$)	Reduced volume ($cm^3 \cdot g^{-1}$)
TS-1-100	-	-	0.156	-
Au/TS-1-100	0.10	10	0.125	0.032
TS-1-35	-	-	0.162	-
Au/TS-1-35	0.10	6	0.141	0.021

[a] Micropore volume (V_{MP}) is estimated by t-plot method.

Figure captions:

Fig. 1 UV-vis spectra of Au solution at different pH (a) and at different time while keeping pH at 7.3-7.5 (b).

Fig. 2 The lowest energy conformations of $[AuCl_4]^-$ (a), $[AuCl_3(OH)]^-$ (b), $[AuCl_2(OH)_2]^-$ (c), $[AuCl(OH)_3]^-$ (d) $[Au(OH)_4]^-$ (e) and $Au(OH)_3$ (f) determined by quench molecular dynamics simulations.

Fig. 3 XRD patterns (a), N_2 adsorption-desorption isotherms (b), FT-IR spectra (c) and UV-vis spectra (d) of TS-1(35) and TS-1(100) supports. The inset in Fig. 3b shows the NL-DFT pore size distributions of the two supports.

Fig. 4 PO formation rate of Au/TS-1 catalysts at different lengths of aging time.

Fig. 5 Representative HRTEM images of the used Au/TS-1(100) catalysts with different lengths of aging time of 4 (a), 18 (b) and 24 h (c) at 200 ^oC, and the particle size distributions of the Au catalysts (d).

Fig. 6 Illustration of the locations of Au particles on Au/TS-1(100) and Au/TS-1(35) catalysts.

Fig. 7 PO formation rate of 0.10 wt% Au/TS-1(35) and 0.10 wt% Au/TS-1(100) catalysts as a function of time-on-stream.

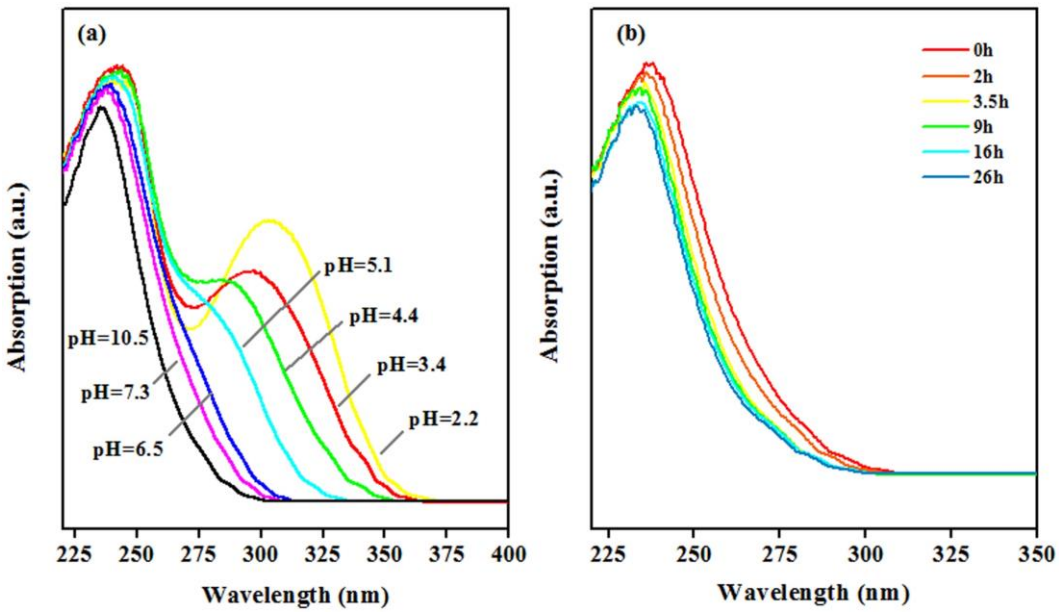

Fig. 1 UV-vis spectra of Au solution at different pH (a) and at different time while keeping pH at 7.3-7.5 (b).

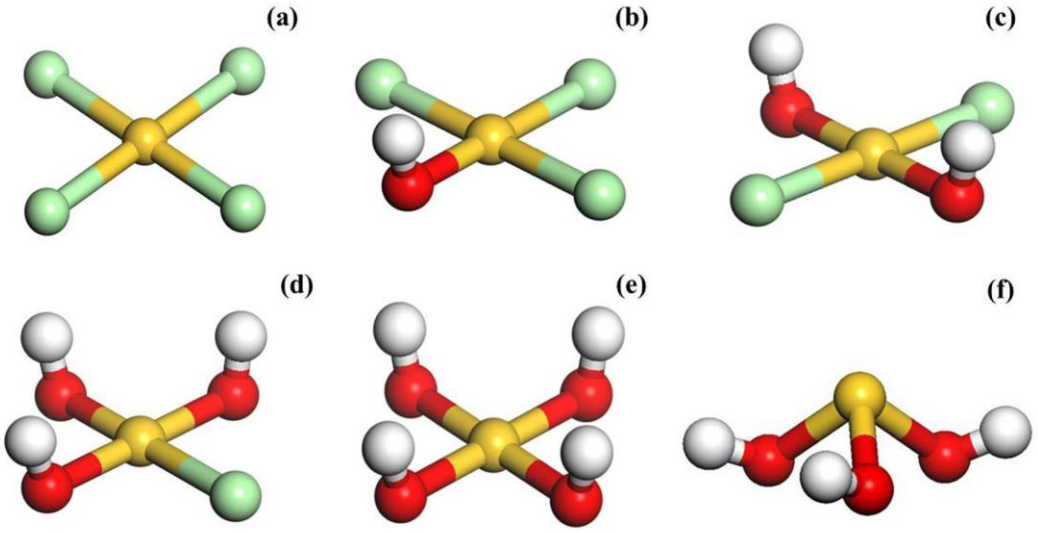

Fig. 2 The lowest energy conformations of $[AuCl_4]^-$ (a), $[AuCl_3(OH)]^-$ (b), $[AuCl_2(OH)_2]^-$ (c), $[AuCl(OH)_3]^-$ (d) $[Au(OH)_4]^-$ (e) and $Au(OH)_3$ (f) determined by quench molecular dynamics simulations.

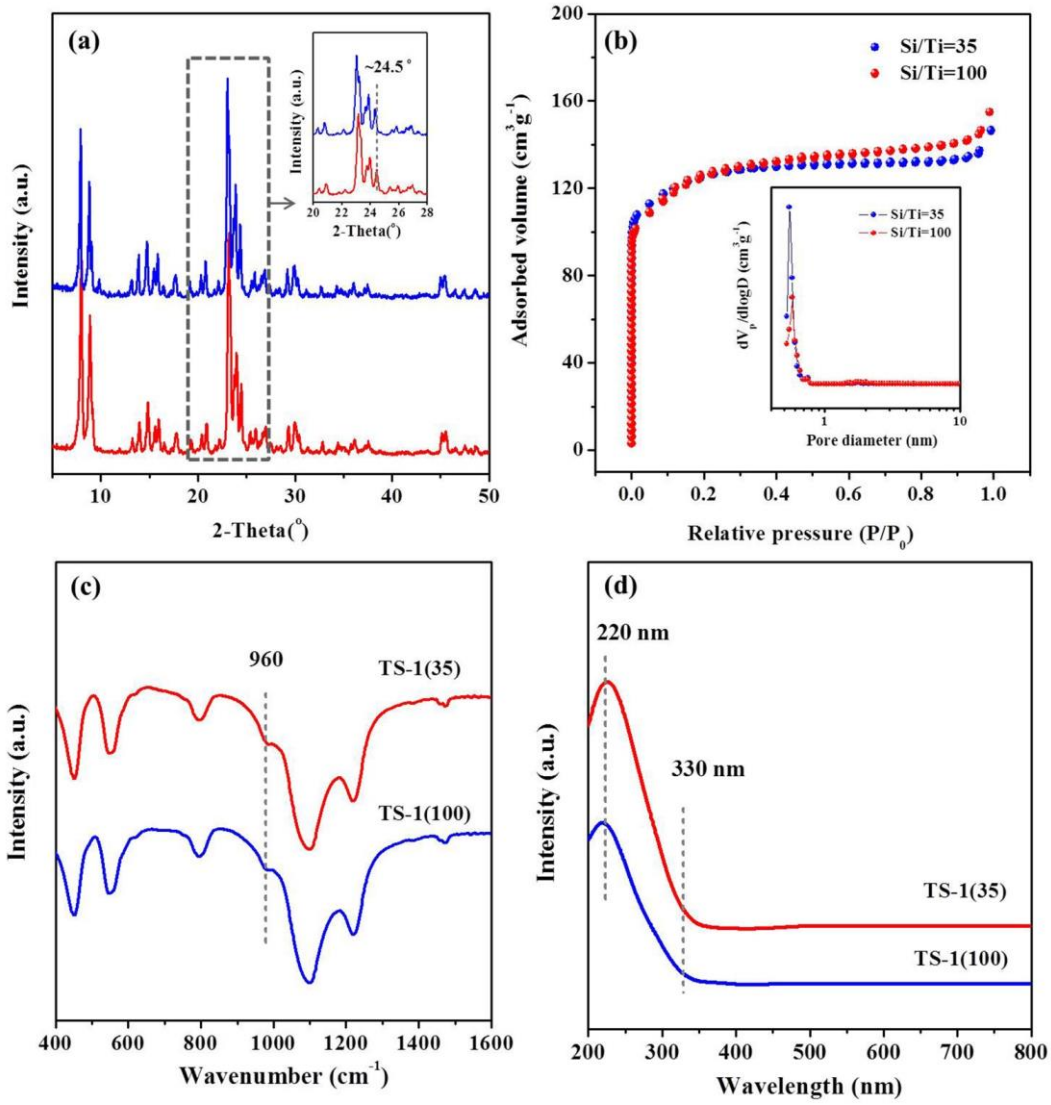

Fig. 3 XRD patterns (a), N_2 adsorption-desorption isotherms (b), FT-IR spectra (c) and UV-vis spectra (d) of TS-1(35) and TS-1(100) supports. The inset in Fig. 3b shows the NL-DFT pore size distributions of the two supports.

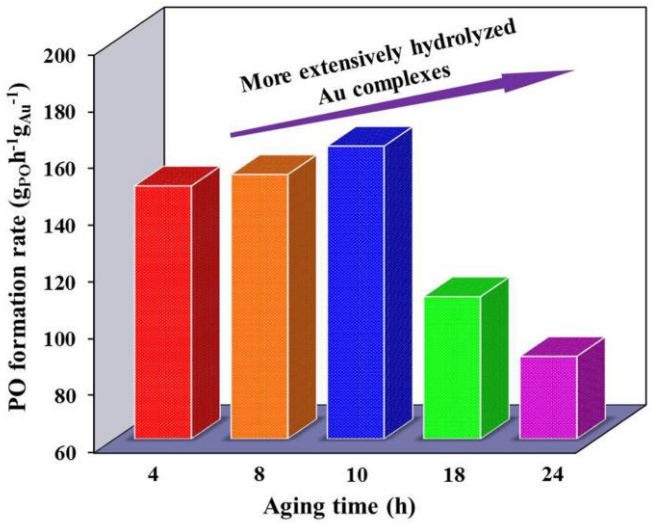

Fig. 4 PO formation rate of Au/TS-1 catalysts at different lengths of aging time.

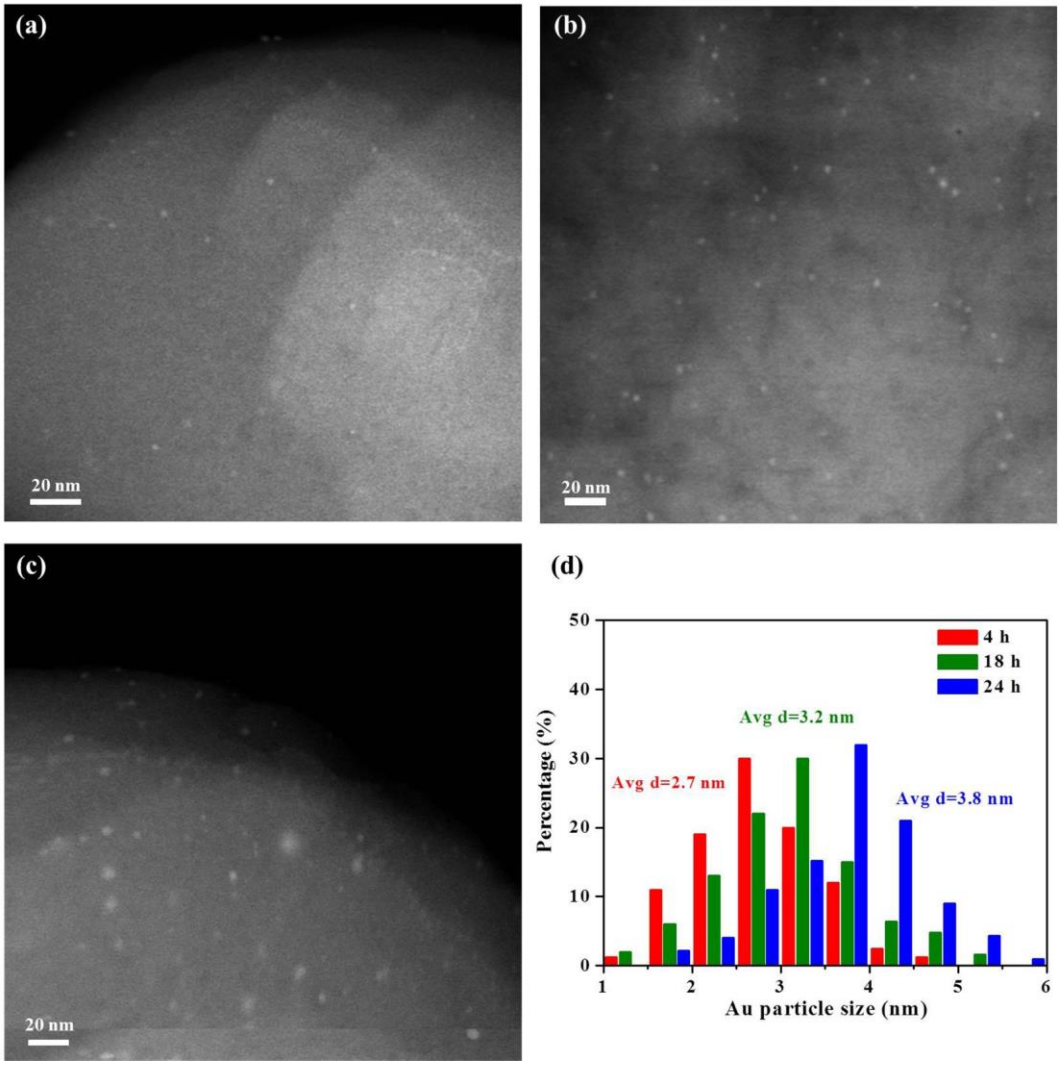

Fig. 5 Representative HRTEM images of the used Au/TS-1(100) catalysts with different lengths of aging time of 4 (a), 18 (b) and 24 h (c) at 200 ºC, and the particle size distributions of the Au catalysts (d).

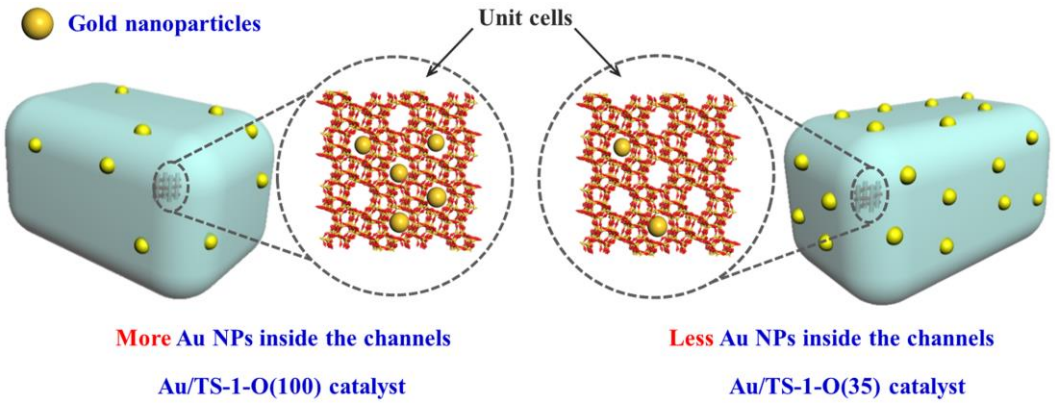

Fig. 6 Illustration of the locations of Au particles on Au/TS-1(100) and Au/TS-1(35) catalysts.

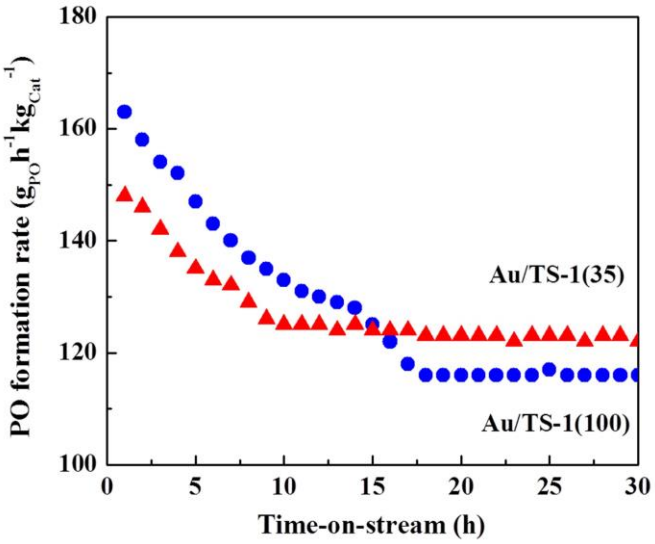

Fig. 7 PO formation rate of 0.10 wt% Au/TS-1(35) and 0.10 wt% Au/TS-1(100) catalysts as a function of time-on-stream.